Relative Humidity as an Indicator for Cloud Formation over Heterogeneous Land Surfaces

CHIEL C. VAN HEERWAARDEN AND JORDI VILÀ-GUERAU DE ARELLANO

Meteorology and Air Quality Section, Wageningen University, Wageningen, Netherlands

(Manuscript received 17 August 2007, in final form 28 February 2008)

ABSTRACT

The influence of land surface heterogeneity on potential cloud formation is investigated using relative humidity as an indicator. This is done by performing numerical experiments using a large-eddy simulation model (LES). The land surface in the model was divided into two patches that had the same sum of latent and sensible heat flux but different Bowen ratios to simulate heterogeneous land surfaces. For heterogeneity in the meso-γ scale (2–20 km), sensitivity analyses were carried out on the heterogeneity amplitude (Bowen ratio difference between contrasting areas) and the inversion strength of potential temperature and specific humidity. The competition between absolute temperature decrease by ABL growth and dry air entrainment in heterogeneous conditions is analyzed using the LES results. First, it is shown that entrainment is located and enhanced over patches with higher Bowen ratios (warm patches) than their surroundings (cold patches). The heterogeneity-induced strong thermals can further penetrate the inversion at the ABL top, thereby reaching lower absolute temperatures than in homogeneous conditions. Second, because of the heterogeneity-induced circulations the moisture is located over the warm patch, and higher time-averaged RH values at the ABL top (RH_{zi}) than over the cold patches are found here, even for dry atmospheres. These RH_{zi} exceed values found over homogeneous land surfaces and are an indication that surface heterogeneity may facilitate cloud formation. In vertical profiles of RH, few differences are found between the homogeneous and heterogeneous cases, but the essential heterogeneity-induced modifications are within the domain variability.

1. Introduction

Convective cloud formation over land is a complex phenomenon caused by the strong interaction between the land surface and the atmospheric boundary layer (ABL; Freedman et al. 2001; Kang et al. 2007). Previous studies (e.g., Ek and Mahrt 1994; Ek and Holtslag 2004) described the underlying physics of these interactions over homogeneous land surfaces. However, it has been suggested (e.g., Crook 1996; Pielke 2001; Kang et al. 2007) that the timing and location of cloud formation are sensitive to heterogeneous forcings at the land surface, which depend on the spatial variability of land use, soil moisture content, and topography.

Heterogeneous forcings occur over a wide range of scale levels, but the strongest effects on ABL properties are found when the heterogeneities are in the meso-γ scale (2–20 km) (Mahrt 2000) because they modify the horizontal and vertical structure of the ABL by inducing circulations. A consequence is that the effects of heterogeneity-induced circulations are difficult to represent well in mesoscale and large-scale models because these flows are mostly in the subgrid scales of the models. To date we lack adequate parameterizations because the effects of circulations on cloud formation in the meso-γ scale are not fully understood.

For scale levels smaller and larger than the meso-γ scale, there is observational and modeling evidence that convective cloud formation and precipitation are enhanced by heterogeneous forcings (e.g., Pielke 2001; Chagnon et al. 2004; Chagnon and Bras 2005; Kang et al. 2007). However, these scales differ from the meso-γ scale because the smaller-scale heterogeneities blend in the surface layer and their effects can be introduced by altering the surface parameters, whereas the larger-scale heterogeneities blend above the ABL and induced motions can be resolved well by mesoscale models (Mahrt 2000).

A key tool for simulating the effects of surface het-

Corresponding author address: Chiel C. van Heerwaarden, Wageningen University, P.O. Box 47, 6700 AA Wageningen, Netherlands.
E-mail: chiel.vanheerwaarden@wur.nl

DOI: 10.1175/2008JAS2591.1

erogeneity on the ABL is a large-eddy simulation (LES) model, which can resolve the most relevant scales of turbulent atmospheric flows (e.g., Moeng 1984). Previous studies (e.g., Hechtel et al. 1990; Hadfield et al. 1991; Avissar and Schmidt 1998, hereafter AS98; Letzel and Raasch 2003; Patton et al. 2005, hereafter PSM05) used the LES technique to investigate the properties of the heterogeneously forced ABL. They explained that circulations can be induced by heterogeneous forcings and demonstrated the dependence of these circulations on the length scale and the amplitude of the heterogeneity. There is agreement on the existence of a typical length scale (a sequence of one cold and warm patch) at which the ABL is modified the most. According to AS98, this scale is 5–10 km, whereas PSM05 formulate this range as 5–8 times the boundary layer height. The precise effects of amplitude (heat flux difference between different patches at the land surface) are not well understood (Mahrt 2000). On the basis of these conclusions, we take the heterogeneity length constant in our study and perform a sensitivity analysis on the heterogeneity amplitude. In this study, we define the amplitude as the difference in Bowen ratio between two patches.

Our study focuses on the role of heterogeneous land surfaces in the formation of convective clouds in the meso-γ scale. Avissar and Liu (1996) found an enhancement of clouds and precipitation on this scale with a mesoscale model. However, Mahrt (2000) showed that for these models the surface-layer parameterizations are not valid over heterogeneous landscapes because induced circulations are not resolved well. Furthermore, PSM05 illustrated the failure of free convective scaling laws over a heterogeneous land surface. The computer power we have available today allows for an LES study at high resolution, in which the flow, including the entrainment processes, is dynamically resolved (Sullivan et al. 1998; Pino et al. 2003). In contrast to Avissar and Liu (1996), we did not study cloudy boundary layers; rather, we focus on the use of relative humidity at the ABL top (RH_{zi}) as an indicator for cloud formation (Ek and Mahrt 1994). Based on the general structure changes as shown by PSM05 and AS98, we study the key elements of the boundary layer dynamics over a heterogeneous surface that defines RH_{zi}.

A process that merits special attention in the evolution of RH_{zi} is the entrainment of warm and dry air from the free atmosphere into the ABL, which influences both boundary layer growth and the thermodynamic structure of the ABL. Ek and Mahrt (1994) studied the role of entrainment on RH_{zi} in a bulk model and showed that the evolution of RH_{zi} is a complex competition between the absolute temperature decrease and the drying effect of ABL growth via entrainment and of surface heating and evaporation. They found that the relative magnitudes of the involved processes are largely dependent on the potential temperature and moisture discontinuities in the inversion layer. Here, we extend the previous work to heterogeneous land surfaces. The effects of heterogeneous forcings on entrainment are still under debate; according to AS98 and Letzel and Raasch (2003), entrainment is enhanced by heterogeneous forcings, whereas PSM05 found no evidence for this. Therefore, we begin our research by investigating entrainment over heterogeneous landscapes, prior to analyzing the heterogeneity-induced changes on the moisture structure of the ABL top.

This first part of this paper is devoted to a study of the influence of the heterogeneity amplitude on the entrainment processes and the boundary layer height. Although AS98, Letzel and Raasch (2003), and PSM05 have already concluded that ABLs are higher over warm patches than over cold patches, the precise role of heterogeneity amplitude and its influence on entrainment processes remain open. Here, we address these issues by studying the spatial distribution of entrainment and comparing the total entrainment for cases with varying heterogeneity amplitudes and inversion strengths for potential temperature and specific humidity. By applying a statistical decomposition between turbulent and mesoscale components, we investigate the contribution of the heterogeneity-induced circulation to entrainment.

In the second part of this paper, we connect our findings about the ABL height and entrainment processes to the thermodynamic changes in the ABL by studying the specific humidity and the RH. We analyzed the spatial structure of temperature, moisture, and RH near the top of the ABL for different heterogeneity amplitudes and inversion strengths of potential temperature and specific humidity. Vertical profiles of the RH and the variances of potential temperature and specific humidity were analyzed to study the modification of the horizontally averaged profiles by heterogeneous forcings. Here, we attempt to generalize the results of the different initial conditions to conclude whether, and in which conditions, land surface heterogeneity influences the RH and if this is beneficial for cloud formation.

2. Methods

a. Model description

The study is based on numerical experiments performed using the Dutch Atmospheric LES (DALES) model, which was initially developed by Nieuwstadt and

TABLE 1. Four regimes in the relative humidity evolution in the entrainment zone, defined by the initial jump conditions.

	$\Delta\theta = 2.0$ K	$\Delta\theta = 0.5$ K
$\Delta q = 0$ g kg^{-1}	(1) Small cooling rate little dry air entrainment	(2) Large cooling rate, little dry air entrainment
$\Delta q = -4$ g kg^{-1}	(3) Small cooling rate, modest dry air entrainment	(4) Large cooling rate, extensive dry air entrainment

Brost (1986), improved by Cuijpers and Duynkerke (1993), and updated to a parallel-processing version by Dosio et al. (2005). DALES solves the filtered Navier–Stokes equations with the Boussinesq approximation applied.

In this study, we introduce a fundamental modification to the DALES code by implementing a third-order Runge–Kutta time integration scheme combined with a fifth-order advection scheme (Wicker and Skamarock 2002). This scheme more accurately resolves steep gradients that are characteristic for the ABL top, which allows for an improved simulation of the finescale entrainment processes.

DALES has periodic boundary conditions in the horizontal plane. At the land surface, the surface fluxes for heat $\overline{w'\theta'}$ and moisture $\overline{w'q'}$ and the friction velocity u_* are prescribed. There is a sponge layer in the top of the model, which prevents the reflection of gravity waves back into the model domain.

b. Experimental setup

For this study we discretized our LES domain into $256 \times 192 \times 192$ grid cells on the x, y, and z axes. The grid length is 25 m in x and y and 12.5 m in z; our domain is thus $6400 \times 4800 \times 2400$ m. According to Bretherton et al. (1998), our vertical resolution is sufficient to resolve most of the scales in the entrainment process. All cases are dry convective boundary layers with prescribed surface heat fluxes. There is no background wind ($U_g = V_g = 0$ m s^{-1}) and the friction velocity u_* is fixed at 0 m s^{-1} (i.e., free local convection). The initial profiles and surface forcings correspond to the temperature and moisture conditions of a typical early summer day in the Netherlands. All simulations have an initial potential temperature profile that is constant with height for the first 800 m. On top of this layer we prescribe a temperature jump (case dependent), and after this jump the stratified free atmosphere has a temperature lapse rate equal to 0.006 K m^{-1}. The initial specific humidity profile in the mixed layer is constant with height (0.005 kg kg^{-1}), with a jump on top of the mixed layer and a constant value in the free atmosphere (case dependent).

The selected value for the potential temperature jump ($\Delta\theta$) determines the growth rate of the ABL. In case of a small jump, the ABL grows fast, and because of the pressure decrease at the top, the ABL top cools in terms of absolute temperature, which has a positive effect on the RH_{zi}. On the other hand, if the jump is small, a large amount of free atmospheric air enters the ABL. For this air, the specific humidity jump (Δq) determines the dryness and thus to what extent the cooling can be compensated for by drying. To simulate all combinations, we classified the initial conditions in four regimes (see Table 1).

To create heterogeneous forcings, the land surface is divided in two parts along the x axis. All grid cells in the left patch (cells 1 to 128) are characterized by a Bowen ratio below the average Bowen ratio (the cold patch) and the cells in the right patch (grid cells 129 to 256) have an above-average Bowen ratio (the warm patch). The length of the heterogeneity (one cycle of a cold and a warm patch) is therefore 6400 m. Because the ABL heights vary between 1000 and 1100 m, the ratio between the heterogeneity length and the ABL height is in the range that AS98 and PSM05 specify for the strongest mesoscale contribution to the flow.

For regime 1 (see Table 1), we performed a sensitivity analysis on the heterogeneity amplitude, which is defined as the Bowen ratio difference between the cold and the warm patches. In all cases, for every location at the land surface, the sensible H and latent LE heat flux add up to 360 W m^{-2}, but the Bowen ratios for the cold and the warm patch differ among the simulations (see Table 3). For the three other regimes we simulated the homogeneous and the largest-amplitude case.

To verify if our results are sensitive to the model domain, we simulated two additional cases based on cases 1 and 5 in which the domain is twice as long (512 cells in x, thus 12 800 m). In this setup the heterogeneous case consists of four patches (see the "large" cases in Table 2 and Table 3).

All cases were initially integrated for 3 h. After this period a quasi-steady state was reached for all cases. We define a quasi-steady state as a situation in which the ABL-averaged turbulent kinetic energy (TKE) normalized by Deardorff's convective velocity scale w_*^2 is constant in time (PSM05). After 3 h of spinup, the three components of the wind, the potential temperature, and specific humidity were recorded for each grid cell every 5 s for 1 h. The statistics are thus based on 720 time steps.

TABLE 2. Initial conditions for all LES simulations; θ_{ML} is the initial mixed layer potential temperature, $\Delta\theta$ is the temperature jump at 800 m, and Δq is the temperature jump at 800 m; regimes follow from Table 1.

Simulation	θ_{ML} (K)	$\Delta\theta$ (K)	Δq (kg kg^{-1})	Regime
Case 1	293.0	2.0	0.000	1
Case 2	293.0	2.0	0.000	1
Case 3	293.0	2.0	0.000	1
Case 4	293.0	2.0	0.000	1
Case 5	293.0	2.0	0.000	1
Case 1 (weak)	294.5	0.5	0.000	2
Case 5 (weak)	294.5	0.5	0.000	2
Case 1 (dry)	293.0	2.0	−0.004	3
Case 5 (dry)	293.0	2.0	−0.004	3
Case 1 (weak–dry)	294.5	0.5	−0.004	4
Case 5 (weak–dry)	294.5	0.5	−0.004	4
Case 1 (large)	293.0	2.0	0.000	1
Case 5 (large)	293.0	2.0	0.000	1

c. Statistical methods

To calculate the turbulent statistics of our model runs we used a method based on phase averaging (Hussain and Reynolds 1970). A similar method was previously employed in the LES study of heterogeneous land surfaces by PSM05. Our model forcings are heterogeneous only on the x axis and thus homogeneous on the y axis. Therefore, we assume that a local spatial average can be calculated by averaging over y. We decompose an arbitrary space- and time-dependent turbulent variable $\phi_{x,y,z,t}$ in two components:

$$\phi_{x,y,z,t} = \langle\phi\rangle_{x,z,t} + \phi'_{x,y,z,t}. \quad (1)$$

We name the first term on the right-hand side the local average, which is the spatial average of all values on the y axis that share the same x, z, and t coordinates. Under homogeneous conditions, $\langle\phi\rangle_{x,z,t}$ equals the slab average because there are no variations in local spatial averages in a horizontal plane. The difference between the local average and the slab average is thus a measure of advection and therefore of the contribution of the heterogeneous surface forcings to the statistics. This contribution we call the mesoscale component from now on. The turbulent fluctuation $\phi'_{x,y,z,t}$ is the second term. In the further analyses we denote spatial averages in the y direction as $\langle\phi\rangle$ and in the x direction as $[\phi]$. Temporal averages are denoted as $\overline{\phi}$.

3. Results

a. Entrainment processes and ABL growth

1) STRUCTURE OF THE ABL TOP AND ENTRAINMENT

Our first objective was to study the influence of the heterogeneity amplitude on entrainment processes and on the evolution of the ABL height. Figure 1 shows the 1-h-averaged ABL height as a function of space along the x axis. The heights are derived using the maximum potential temperature gradient following the procedure in Sullivan et al. (1998). For every x, y coordinate the ABL height is calculated for each time step, and these values are averaged over y and time. The values in the figure are scaled by the horizontally averaged ABL height.

Figure 1 shows that the presence of horizontal variability in the surface forcings results in a spatial variability of the ABL height z_i along the heterogeneity. The homogeneous case (case 1) has an ABL height that is $z/z_i = 1.0$ with small fluctuations around this value, whereas in all heterogeneous cases a clear spatial pattern is visible, with a deeper boundary layer over the warm patch. Therefore, we corroborate the earlier find-

TABLE 3. Surface boundary conditions for all LES simulations; H_L is the sensible heat flux of the cold patch, H_R is the sensible heat flux of the warm patch, LE_L is the latent heat flux of the cold patch, LE_R is the latent heat flux of the warm patch, β_L is the Bowen ratio of the cold patch, and β_R is the Bowen ratio of the warm patch.

Simulation	H_L (W m^{-2})	H_R (W m^{-2})	LE_L (W m^{-2})	LE_R (W m^{-2})	β_L	β_R
Case 1	120	120	240	240	0.50	0.50
Case 2	105	135	255	225	0.41	0.60
Case 3	90	150	270	210	0.33	0.71
Case 4	75	165	285	195	0.26	0.85
Case 5	60	180	300	180	0.20	1.00
Case 1 (weak)	120	120	240	240	0.50	0.50
Case 5 (weak)	60	180	300	180	0.20	1.00
Case 1 (dry)	120	120	240	240	0.50	0.50
Case 5 (dry)	60	180	300	180	0.20	1.00
Case 1 (weak–dry)	120	120	240	240	0.50	0.50
Case 5 (weak–dry)	60	180	300	180	0.20	1.00
Case 1 (large)	120	120	240	240	0.50	0.50
Case 5 (large)	60	180	300	180	0.20	1.00

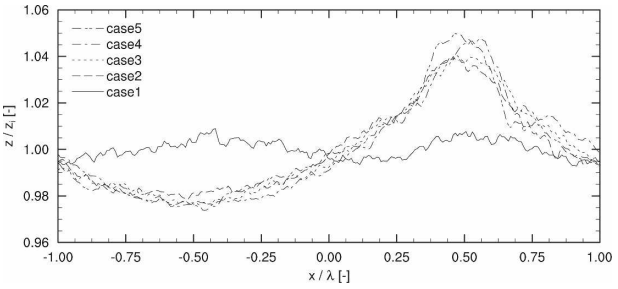

FIG. 1. Averaged ABL height along the x coordinate during 1 h. Horizontal coordinates are scaled by the patch size λ; vertical coordinates are scaled by the time and area-averaged ABL height $[\overline{\langle z_i \rangle}]$.

ings of AS98 and PSM05, who showed ABL height variations for different heterogeneity lengths.

Slight variations in this pattern are visible, caused by differences in the heterogeneity amplitude. For instance, above the warm patch ($x/\lambda = 0.5$), there is an increase in ABL height related to the larger heterogeneity amplitude. Case 2 has a height that is 4% larger than the average ABL height ($z/z_i = 1.04$), whereas case 5 attains values up to 5% larger ($z/z_i = 1.05$) than the average. Over the cold patch, the opposite effect is visible, with a decreasing ABL height for increasing heterogeneity amplitude. In spite of the small variations caused by the heterogeneity amplitude, the main variations in ABL height are due solely to the presence of a heterogeneity-induced circulation. For cases with weak inversions (not shown), we found for case 5 (dry) the same relative increase over the warm patch ($z/z_i = 1.05$).

Figure 2 shows the spatial distribution of entrainment and contains the cross sections of the 1-h averaged values of the normalized turbulent heat flux $\overline{\langle w'\theta_v' \rangle}/[\overline{\langle w'\theta_v' \rangle}_0]$ for cases 2 and 5. The overlying vector plot shows the wind that is driven by the differential heating of the domain. Before analyzing the figure, it is worth mentioning that the average subgrid scale contribution to the heat flux at $z/z_i = 0.95$ is 5.6% for case 5 (subgrid flux 0.0011 K m s^{-1}; resolved 0.0183 K m s^{-1}), which indicates that the resolved part largely exceeds the subgrid part and thus that the flow is resolved accurately.

A stronger heterogeneity amplitude results in stronger surface winds toward the center of the warm patch where thermals are merged. Case 2 has, for instance, a wind of approximately 1 m s^{-1} at $x/\lambda = 0.3$ and $z/z_i = 0.05$, whereas case 5 has more than 2 m s^{-1} at the same location. The strongly buoyant thermals that are the product of the merging can penetrate the entrainment zone more vigorously, thereby locally enhancing entrainment, for instance at $x/\lambda = 0.5$ and $z/z_i = 1.0$. The normalized entrainment minima found for case 2 are −0.4 and −0.6 times the surface flux, whereas in case 5

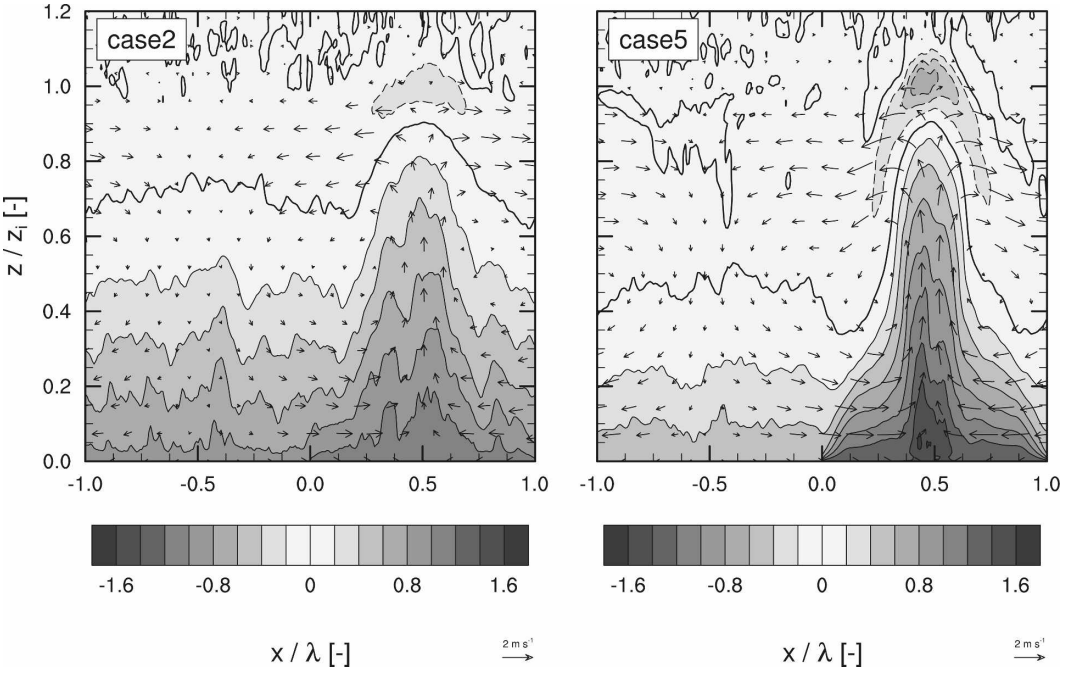

FIG. 2. Cross section of the 1-h-averaged normalized turbulent heat transport $\overline{\langle w'\theta_v' \rangle}/[\overline{\langle w'\theta_v' \rangle}_0]$ for cases (left) 2 and (right) 5. Vectors indicate the wind direction and magnitude. The horizontal coordinates are scaled by the patch size λ and the vertical coordinates are scaled by the ABL height $[\overline{\langle z_i \rangle}]$.

the values have a range from −0.8 to −1.0 times the surface flux. These local values largely exceed the ratio of −0.2 times the surface flux that is widely used in parameterizations of the entrainment flux. Although the ABL heights over the warm patch are only slightly sensitive to heterogeneity amplitude, the entrainment minima increase greatly with increasing amplitude. In the next section we discuss the effects of this local entrainment enhancement on the total area-averaged entrainment over the heterogeneous land surfaces.

In contrast to the warm patch, over the cold patch thermals are suppressed by the downward wind of the induced mesoscale circulation (downward motions $x/\lambda = -1.0$ to 0.0). At the top of the ABL winds are directed toward the cold patch ($x/\lambda = 0.2$ and 0.8). Convergence of air occurs here and the warm air is advected downward toward the land surface. This downward-moving warm air does not allow thermals generated over the cold patch to reach the ABL top and thereby prevents entrainment over the cold patch. The line at which the turbulent flux becomes zero is located at $z/z_i = 0.7$ for case 2 and at $z/z_i = 0.5$ for case 5. The suppression of upward-moving thermals is thus enhanced as heterogeneity amplitude increases. Above the warm patch we find strong upward motions (more than 3 m s^{-1} for case 5) over a small area, whereas the cold patch has gentle downward motions (less than 1 m s^{-1}) over the whole cold patch. We discuss now how the temperature at the ABL top is influenced by the modified entrainment.

Figure 3 shows the 1-h-averaged space-dependent values for the potential temperature and the absolute temperature near the top of the ABL. The potential temperature is nearly uniform in case 1 as expected, although there are some fluctuations that are the result of the domain size. For all heterogeneous cases, the potential temperature at $x/\lambda = 0.5$ (core of the thermals) has a range of values approximating 295.1 K. These values are colder than their surroundings because the thermals have become negatively buoyant in the temperature inversion. As shown in Fig. 2, at the top of the ABL the entrained air is horizontally advected to the cold patch. The entrainment events are very well visible in case 5, with the two temperature peaks of 295.7 K at $x/\lambda = 0.25$ and $x/\lambda = 0.75$, caused by the warm free tropospheric air that is being engulfed into the ABL.

The absolute temperature at the top of the ABL shows more variation than the potential temperature because of the variation in boundary layer height over the patches (see Fig. 1). Although the rising thermals for the heterogeneous cases at $x/\lambda = 0.5$ have comparable potential temperatures at the ABL top, their

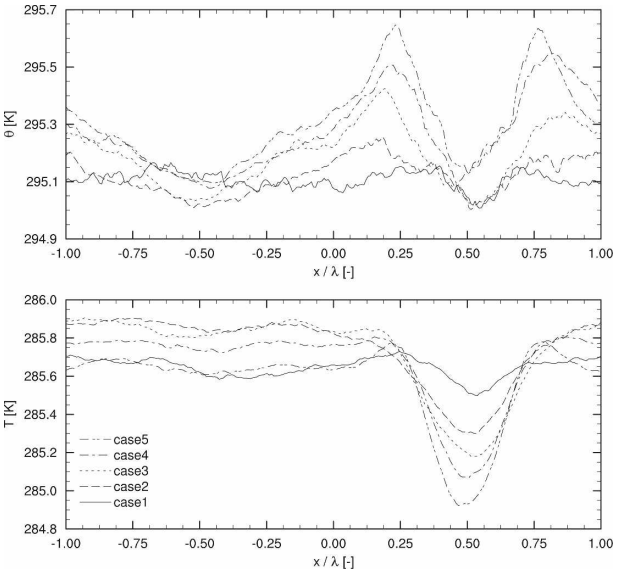

FIG. 3. One- hour averaged (top) potential and (bottom) absolute temperature along the x axis at $z/z_i = 0.95$. Horizontal coordinates are scaled by the patch size λ.

absolute temperatures decrease if the heterogeneity amplitude increases. The homogeneous case 1 has an absolute temperature of 285.5 K, whereas the temperature here gradually decreases as heterogeneity amplitude becomes larger. For the strongest amplitude case (case 5), we find an absolute temperature of 284.9 K. In consequence, under the assumption of equal moisture conditions, the relative humidity will increase for larger heterogeneity amplitudes. In cases characterized by weaker inversions (smaller temperature jump at the ABL top), we found identical variation in the ABL height within the domain (not shown) and therefore the entrainment zone has a similar absolute temperature variability. The fact that weaker inversions do not yield a larger variability in ABL height and temperature may be explained by the nature of the motions in the entrainment zone in these conditions. If the inversion is weak, folding of the interface between the ABL and the free atmosphere occurs and these types of motions are associated with larger horizontal spatial scales rather than entrainment events in strong inversion cases (Sullivan et al. 1998). Therefore, additional ABL height variation in heterogeneous cases with weak inversions may not exist as the effects are spread out in the horizontal.

2) AREA-AVERAGED ABL GROWTH AND ENTRAINMENT

Here, we further discuss the effects of surface variability on the thermodynamic vertical profiles. To ad-

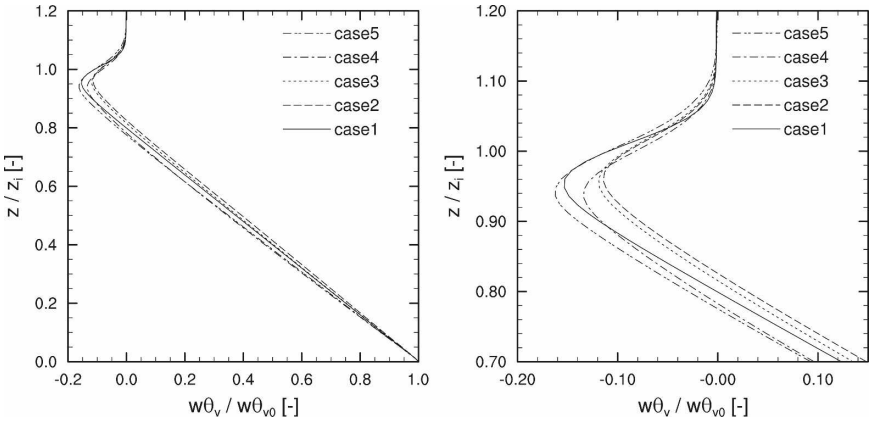

FIG. 4. Vertical profiles of the 1-h-averaged total heat transport $[\overline{w\theta_v}]$. (right) Zoom of (left). Horizontal coordinates are scaled by the surface sensible heat flux $[\langle w'\theta'_v\rangle_0]$; vertical coordinates are scaled by the ABL height $[\overline{\langle z_i\rangle}]$.

dress these effects, the vertical profiles of the homogeneous case 1 are compared with the four heterogeneous cases. Just as a reminder, notice that all cases have the same area-averaged sensible and latent heat fluxes and initial thermodynamic profiles. Consequently, differences among the simulations must be induced by the heterogeneous forcings and by the subsequent local effects on entrainment.

Figure 4 shows the 1-h area-averaged heat flux profiles for all the simulations. In spite of the large structural changes that heterogeneity induces, there are only small differences between the homogeneous and heterogeneous cases, although (as we show later) the distribution between mesoscale and turbulent contributions to the heat flux varies considerably. All cases show a linear heat flux profile in the ABL ($z/z_i = 0$–0.8) and an area of negative heat flux at the top of the ABL that characterizes the entrainment zone ($z/z_i = 0.8$–1.1). The curved profiles of the heat flux that AS98 found for heterogeneous cases are not present in our cases. We found linear profiles similar to those in PSM05. Therefore, we assume that heterogeneous cases should yield linear profiles and that AS98 results are the effect of the low resolution of their model runs.

The region with negative heat flux is a measure of the contribution of entrainment (vanZanten et al. 1999) to the heating of the ABL. This implies that the depth of the entrainment zone δ and the magnitude of the minimum flux both correlate positively with the total entrainment. Compared to the homogeneous case, the two smallest-amplitude cases (cases 2 and 3) have a shallower entrainment zone ($\delta/z_i = 0.85$–1.1) with a lower minimum flux ($\overline{\langle w'\theta'_v\rangle}/\overline{\langle w'\theta'_v\rangle}_0 = -0.12$). The total entrainment of heat for these two cases thus appears to be less than in the homogeneous case 1 ($\delta/z_i = 0.3$, $\overline{\langle w'\theta'_v\rangle}/\overline{\langle w'\theta'_v\rangle}_0 = -0.16$). In the two largest-amplitude cases, the entrainment zone have become larger (both $\delta/z_i = 0.35$) than the homogeneous case, characterized by a larger minimum for case 5 ($\overline{\langle w'\theta'_v\rangle}/\overline{\langle w'\theta'_v\rangle}_0 = -0.16$), which suggests that more heat is entrained in these cases.

Figure 5 shows the temporal evolution of the area-averaged ABL height for all five cases computed following the maximum temperature gradient method (Sullivan et al. 1998). After three hours of spinup, the ABL heights of cases 4 (1000 m) and 5 (1010 m) are the largest, but the growth rate of all five cases, which is the entrainment velocity, has a similar magnitude (approximately 70 m h^{-1}). If all cases have the same entrainment velocity, the entrainment differences found in the previous section cannot exist. Therefore, the suggested enhancement found in Fig. 4 may be the result of the horizontal averaging, where the strongest-amplitude cases have a deeper negative area due to the greater variability in ABL height over the domain. This connects with the findings of Lilly (2002), who suggests that the smooth heat flux profiles in the entrainment zone

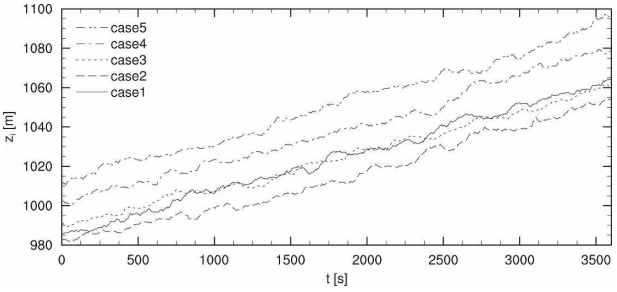

FIG. 5. Domain-averaged ABL height $[\langle z_i\rangle]$ during the hour of data recording for cases 1–5.

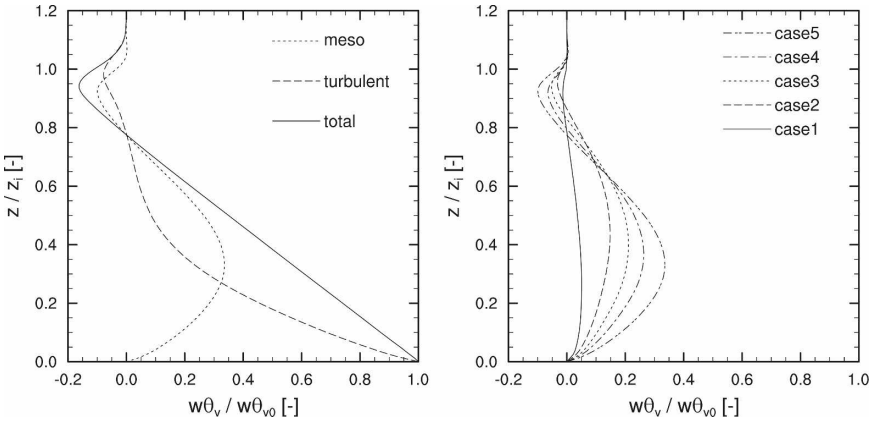

FIG. 6. (left) The horizontally averaged vertical profile of the 1-h-averaged heat transport for case 5 $[\overline{w\theta_v}]$ decomposed into a mesoscale $[\overline{\langle w\rangle\langle\theta_v\rangle}]$ and turbulent contribution $[\overline{\langle w'\theta_v'\rangle}]$. (right) The mesoscale $[\overline{\langle w\rangle\langle\theta_v\rangle}]$ contributions for cases 1–5. Horizontal coordinates are scaled by the surface flux $[\overline{w\theta_{v0}}]$ and the vertical coordinates are scaled by the ABL height $[\overline{\langle z_i\rangle}]$.

found in LES are mostly an effect of horizontal averaging and the that link to the entrainment rate should be made carefully. PSM05 found no significant enhancement of entrainment when they performed a sensitivity analysis of the effect of the heterogeneity length, but they did not vary the heterogeneity amplitude. We showed by varying the amplitude that the results of PSM05 are correct and we thus disagree with previous suggestions of AS98 and Letzel and Raasch (2003) that the area-averaged entrainment is enhanced. Changes in ABL height are the result of the model spinup, and once the model is in quasi-stationary state, the entrainment rate is constant for all heterogeneity amplitudes. Therefore, only the spatial changes will influence the structure of the RH; the spatially averaged ABL growth is not affected.

3) MESOSCALE CONTRIBUTIONS TO ENTRAINMENT

We discussed previously that Fig. 4 showed similar linear heat flux profiles in the ABL for both homogeneous and heterogeneous cases. Nevertheless, there is a fundamental difference between the cases. In the homogeneous case all the heat transport is driven by small-scale turbulence, but in the heterogeneous cases the total heat flux is the sum of the mesoscale and turbulent part that add up to the linear profile. The left-hand side of Fig. 6 shows the decomposition for case 5.

The mesoscale component for the flux is present throughout the whole ABL, but the strongest contributions are found at $z/z_i = 0.3$ for the heat transport, which was also obtained by PSM05. The division between mesoscale and turbulent contributions in the entrainment zone shows that the lower region of the entrainment zone ($z/z_i = 0.8$–0.95) is mostly driven by mesoscale motions, whereas in the top ($z/z_i = 0.95$–1.1) of the entrainment zone the turbulent contribution is the dominant one. Thus, only the strongest engulfing motions reach the lower half of the entrainment zone. Because of the induced circulation, these events are always at the same location (see the peaks in Fig. 3) and are therefore enclosed in the mesoscale contribution. They are associated with large pockets of warm tropospheric air that enter the ABL at the edges of the strong thermals that are pushing the inversion layer. In contrast, the small-scale mixing, quantified by the turbulent part, occurs only at the top of the warm patch, but not at a fixed location. For increasing heterogeneity amplitude, the mesoscale contribution to entrainment increases (see the right-hand side of Fig. 6) as the induced circulation becomes stronger (see wind vectors in Fig. 2).

Case 2 has only $[\overline{\langle w\rangle\langle\theta_v\rangle}]/[\overline{w\theta_{v0}}] = -0.03$, whereas case 5 may even reach $[\overline{\langle w\rangle\langle\theta_v\rangle}]/[\overline{w\theta_{v0}}] = -0.12$. We show in Fig. 6 that these contributions are caused by large-scale entrainment events, which have a fixed location.

b. Relative and specific humidity in the ABL

1) STRUCTURE OF THE SPECIFIC HUMIDITY

In the previous section we focused on the heterogeneity amplitude to study how the strength of the mesoscale circulation influenced entrainment and ABL growth. Now, we discuss the effect of these structure changes on the spatial distribution of specific humidity in the ABL top.

Figure 7 is a 1-h spatially dependent cross section of the specific humidity at $z/z_i = 0.95$. We find that the

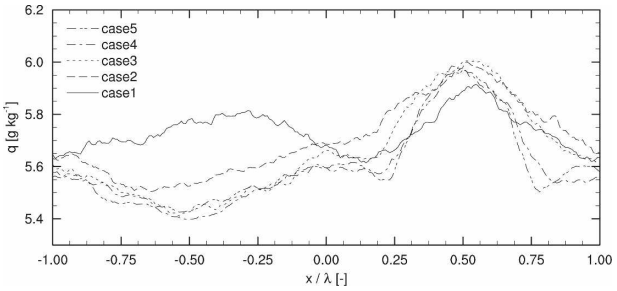

FIG. 7. One-hour-averaged specific humidities q along the x axis. Horizontal coordinates are scaled by the patch size λ.

largest values of the specific humidity are found over the center of the warm patch (6.0 g kg^{-1}). Just as for the potential temperature at z_i, the specific humidity near the ABL top is only slightly dependent on heterogeneity amplitude because the concentration of specific humidity is nearly the same in the rising thermals (6.0 g kg^{-1}) for all heterogeneous cases. The increasing ABL height (see Fig. 1) over the warm patch with increasing amplitude does not influence the specific humidity of the thermals because it is a conservative variable, like potential temperature. The homogeneous case exhibits a large fluctuation, which is a result of the domain size (see the appendix) and of the fact that the scale of moisture fluctuations has a tendency to increase in time (Jonker et al. 1999; De Roode et al. 2004). Therefore, a larger domain in the y axis should yield smaller fluctuations because the mean then consists of multiple cycles of the largest spatial scales.

The low specific humidity at the top of the ABL near the center of the cold patch (5.4 g kg^{-1}) is caused by the entrainment of relatively dry air that is horizontally advected by the mesoscale flow, shown in Fig. 2. The downward transport dries the cold patch from the top, which explains the pocket of dry air that Avissar and Liu (1996) and AS98 found over the cold patch. Thus, the atmosphere over the warm patch is moist, despite the low surface evaporation that characterizes this patch, and the cold patch with the high rate of evaporation is dry. Therefore, the location of the largest moisture content in the ABL top coincides with the location of the lowest absolute temperatures (see Fig. 3) and a situation is created that should result in larger values of RH_{zi} over the warm patch.

The beneficial effect of the heterogeneity-induced moisture transport toward the thermals over the warm patch becomes obvious in a scatterplot of vertical wind speed and specific humidity for case 1 (large) and case 5 (large) (see Fig. 8). This figure contains data from an instantaneous horizontal field taken in the entrainment zone at $z/z_i = 0.95$ during the first time step of the

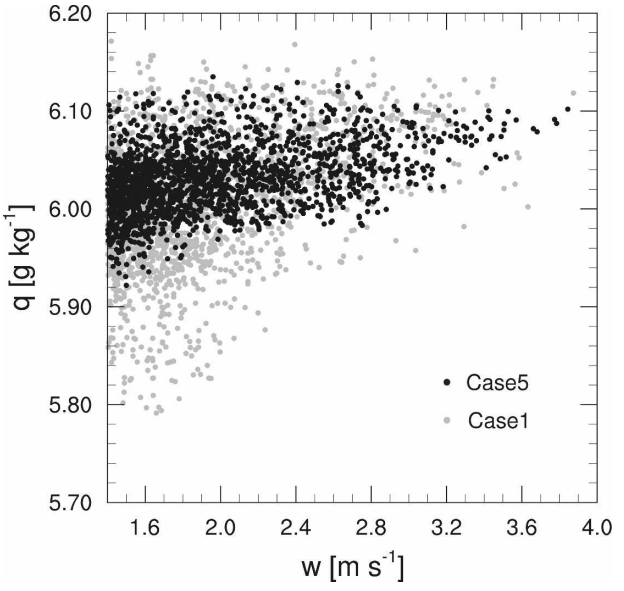

FIG. 8. Scatterplot of vertical wind speeds w larger than 1.4 m s^{-1} vs the specific humidity q at $z/z_i = 0.95$ for case 1 (large) and case 5 (large) during the first time step of data recording.

sampling hour. We have conditionally sampled the vertical wind and the specific humidity for the thermals by taking the area where the vertical velocity exceeds 1.4 m s^{-1}. The plot shows that the thermals for the homogeneous case 1 (large) are on average drier (because there are significantly more points in the range from 5.8 to 6.0 g kg^{-1}) than for the heterogeneous case 5 (large), for which the values of most of the points are slightly larger than 6.0 g kg^{-1}. If we assume that the largest vertical wind speeds are associated with the core of the thermals, then both cases have the same specific humidity in the core (6.05 g kg^{-1} if the wind exceeds 3.0 m s^{-1}). Under the assumption that lower wind speeds occur at the edges of the thermals, we can argue that for this region the heterogeneous case is more efficient in transporting moisture. Because of the merging of thermals by the circulation, the thermals in the heterogeneous case may have a larger ratio of volume to surface and suffer less from drying by detrainment at the side of the thermals. Therefore, in heterogeneous conditions, more moisture reaches the entrainment zone, and thus the RH_{zi} may increase.

2) SPATIAL DISTRIBUTION OF RELATIVE HUMIDITY

Relative humidity is the indicator that links the results of the boundary layer growth and temperature analyses with the findings on the moisture structure. Here, we include the simulations that are performed for the regimes with weaker temperature inversions and a drier upper atmosphere to investigate the importance

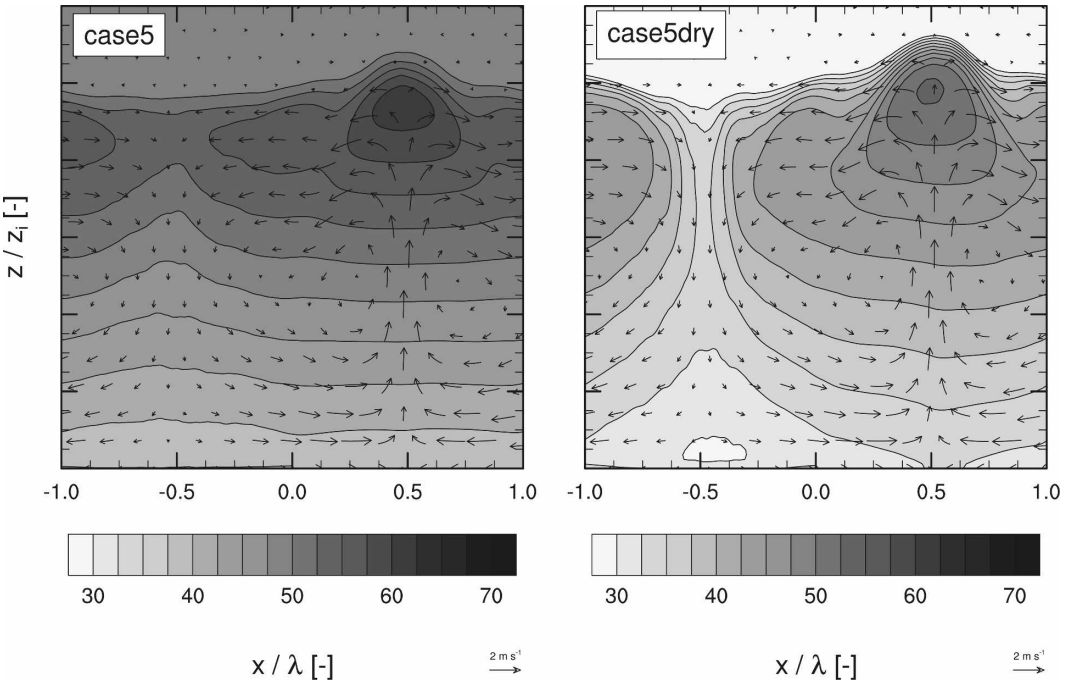

FIG. 9. Cross section of the 1-h-averaged relative humidity $\overline{\langle RH \rangle}$ for (left) case 5 and (right) case 5 (dry). The horizontal coordinates are scaled by the patch size λ and the vertical coordinates are scaled by the ABL height z_i. Vectors indicate the wind direction and magnitude.

of the thermodynamic structure of the entrainment zone. Figure 9 shows the 1-h-averaged cross section of $\overline{\langle RH \rangle}$ for case 5 and case 5 (dry).

For case 5, the ABL top over the warm patch reaches values up to RH = 62.5% ($x/\lambda = 0.5$, $z/z_i = 0.95$), whereas the cold patch does not exceed RH = 55%. At the center of the cold patch, there is a dry area at $x/\lambda = -0.5$, $z/z_i = 0.9$ caused by the entrained dry air that is transported downward here (see vectors in Fig. 9). The structure of case 5 (dry) is similar to case 5 over the warm patch. Despite the dry upper air, there is still an enhanced RH over the center of the warm patch (RH = 55%), but over the cold patch the effect of dry air entrainment is much more profound, with an RH of 30% at the ABL top. Above the center of the cold patch ($x/\lambda = 0.5$), the RH is the minimum for that height. The effects of dry air entrainment extend down to the land surface: the surface RH at $x/\lambda = -0.5$ is less than 30%, whereas over the warm patch at $x/\lambda = 0.5$, the RH exceeds 35%. A comparison of case 5 (weak) and case 5 (weak–dry) yielded similar structures (not shown).

The maximum RH over the warm patch (RH = 62.5%) of case 5 exceeds the value found over a homogeneous land surface sharing the same area-averaged fluxes (RH = 59%; see Fig. 11). In the cases characterized by a drier upper atmosphere, the RH enhancement effect is still important, despite the intense dry air entrainment, because this air is horizontally advected toward the cold patch and does not directly influence the RH over the center of the warm patch (see Fig. 9). Because RH is our chosen indicator for cloud formation (Ek and Mahrt 1994), we therefore expect that in free convective conditions cloud formation may occur earlier over heterogeneous land, independent of temperature and moisture inversion strengths. This finding provides a more complete framework than previous observational and modeling studies (Avissar and Liu 1996; Chagnon et al. 2004) that found that cloud formation is enhanced over areas that are warmer and drier than their environment.

3) VARIABILITY OF AREA-AVERAGED RELATIVE HUMIDITY

Figure 10 shows the 1-h-averaged vertical profiles of the relative humidity. In the left figure, the shaded area is the range of the 1-h-average relative humidities found in case 5, and the hatched area is the range of temporal averaged RHs in case 5 (weak). This figure shows that the mean profiles of RH are nearly identical, with the maximum RH at $z/z_i = 0.95$. The large-amplitude cases are characterized by a deeper entrainment zone (see Fig. 4), which tends to distribute the moisture over a larger region. The RH peak in the

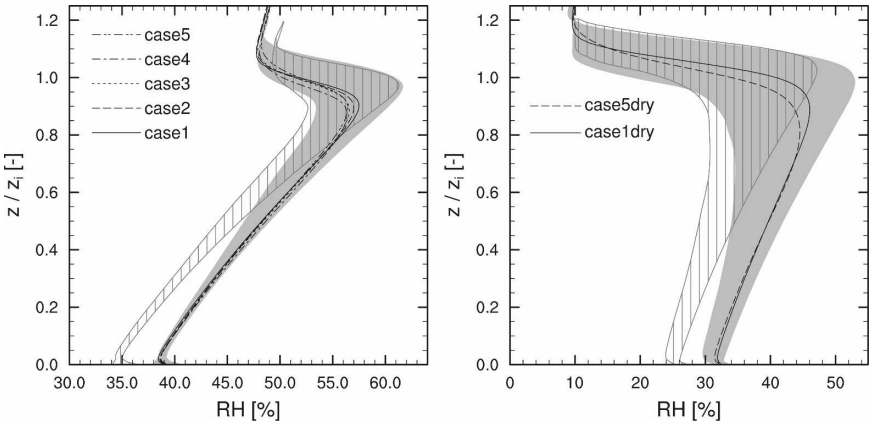

FIG. 10. (left) Vertical profile of the spatial- and time-averaged value of the relative humidity $[\overline{\langle RH \rangle}]$ for all cases. The gray shading shows the range of time-averaged values of relative humidity $\overline{\langle RH \rangle}$ within the domain of case 5. The gray hatched area shows the same range but for case 5 (weak). (right) The $[\overline{\langle RH \rangle}]$ for case 1 (dry) and case 5 (dry), with the variability of case 5 (dry) shaded in gray and of case 5 (weak–dry) hatched.

homogeneous case is thus slightly higher (RH = 57%) than in the heterogeneous cases (RH = 55%). Notice that the area-averaged RH is not enhanced by heterogeneity, which is supported by the fact that we have identical surface fluxes and entrainment velocities for all amplitudes (see Fig. 5).

The large RH-variability of case 5 (gray shaded area) indicates the importance of variability on possible cloud formation. The mean profiles of cases 1 and 5 are very similar, but in case 1 there is hardly any variability within the domain (not shown). In case 5, we find a range of 7% (RH = 54%–61%) within the domain. This variability range is even larger (9%; RH = 52%–61%) if the temperature inversion strength becomes weaker because of the extra dry air entrainment that sinks over the cold patch.

The cases with a dry upper atmosphere (right-hand side of Fig. 10) have a larger range of RH-values in the ABL (as we found in Fig. 9) and again have similar mean profiles. Case 5 (dry) has at $z/z_i = 0.95$ a range of 25% (RH = 25%–50%), whereas the range of case 5 (weak–dry) is 20% (RH = 26%–46%). By comparing the left and right sides of Fig. 10, it becomes clear that the dry upper atmosphere decreases the RH for the whole ABL, but according to the shaded and hatched areas, the effects are mostly noticeable in the RH decrease over the cold patch. For instance, case 5 (dry) has a maximum RH over the warm patch that is approximately 10% lower than case 5 (50% versus 61%), whereas the minimum over the cold patch is approximately 30% less (25% versus 54%) because of the advection of the very dry entrained air to here. An important consequence, therefore, is that even with dry upper atmosphere conditions, the RH over the warm patch is enhanced compared to the homogeneous case sharing the same conditions.

Figure 11 shows the maximum time-averaged $\overline{\langle RH \rangle}$ found in the entrainment zone for all cases. The maximum value of RH increases with heterogeneity amplitude for the four defined regimes of potential temperature and specific humidity inversion strengths. For the numerical experiments with a strong inversion, the values range from 59.4% (case 1) to 61.8% (case 5) for a

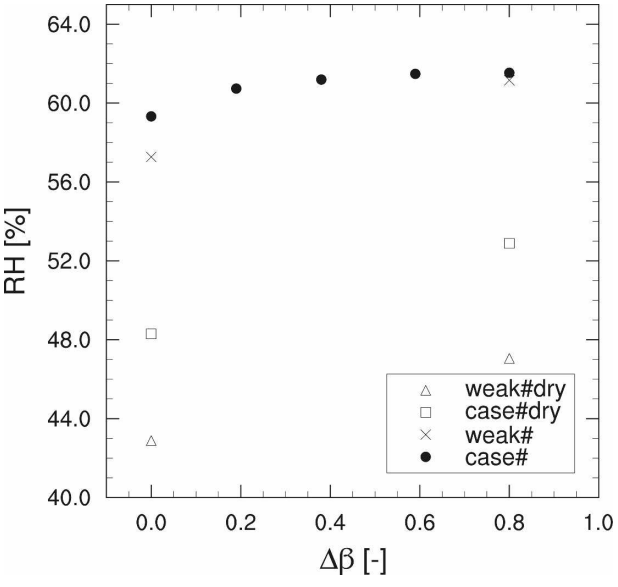

FIG. 11. Relation between the maximum time-averaged relative humidity $\overline{\langle RH \rangle}_{max}$ per domain vs the heterogeneity amplitude $\Delta\beta$ for all regimes.

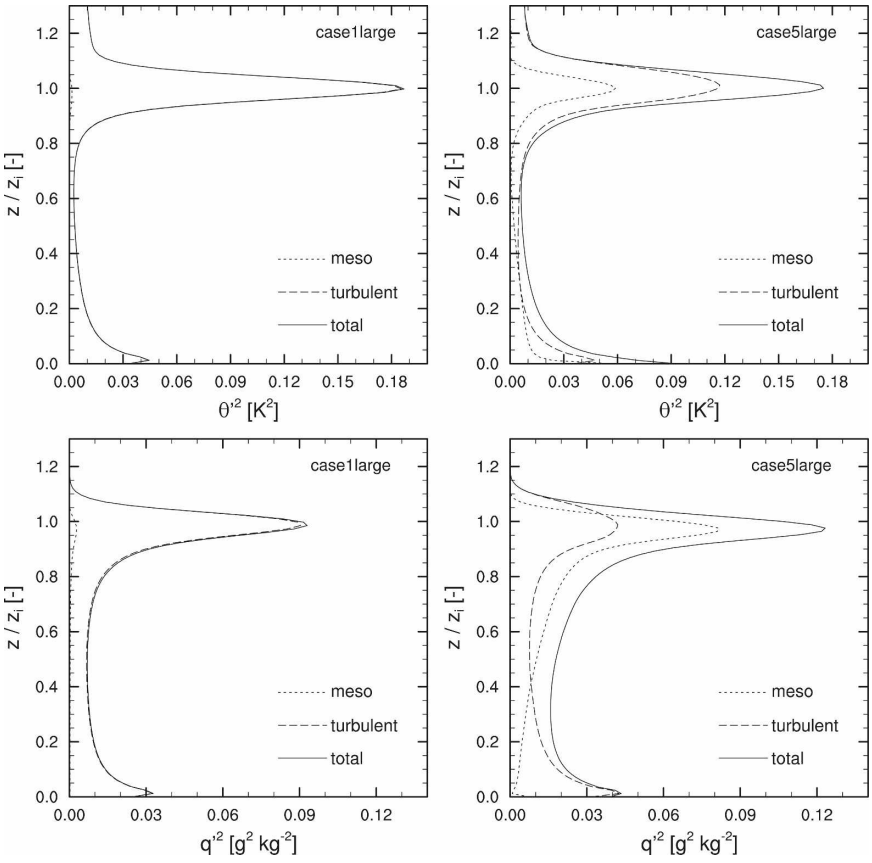

FIG. 12. (top) Vertical profiles of the potential temperature variance for case 1 (large) and case 5 (large) decomposed in mesoscale $[\overline{\langle\theta\rangle^2}] - [\overline{\langle\theta\rangle}]^2$ and turbulent parts $[\overline{\langle\theta'^2\rangle}]$ and their total. (bottom) Decomposed variances and their total of specific humidity for the same cases.

moist upper atmosphere and from 48.5% [case 1 (dry)] to 51.0% [case 5 (dry)] in the dry case. The weak inversion cases show a slightly stronger correlation between the maximum RH and the heterogeneity amplitude [case 1 (weak) = 57.4%, case 1 (weak) = 61.3%, case 1 (weak–dry) = 43.0%, case 5 (weak–dry) = 47.0%], which is in agreement with our previous finding that in weak inversions the ABL height variability is relatively larger compared to the strong inversion cases. Although a difference of 3–4% between the homogeneous and strongest heterogeneous case is small, Ek and Mahrt (1994) found that in the afternoon the typical RH_{zi} tendency per hour has similar values. Therefore, there might be a difference in cloud onset between the homogeneous and heterogeneous cases on the order of an hour, if we take initial conditions for the LES simulations closer to saturation.

4) VERTICAL PROFILES OF VARIANCES

We conclude this study with an analysis of the variances of the potential temperature and specific humidity in the entrainment zone to show that these variables are influenced by the nonuniform forcings at the land surface (see Fig. 12). The first finding we discuss is the creation of mesoscale variance. The figure shows that for potential temperature one-third (0.06 K^2) of the total variance of 0.18 K^2 is in the mesoscale contribution at $z/z_i = 1.0$. Specific humidity at this height has a significantly larger part of the variance in the mesoscale (see bottom right panel in Fig. 12): this contribution is approximately two-thirds of the total [(0.08/0.12) g^2 kg^{-2}]. An explanation for the shift is that in the heterogeneous case, thermals are organized over the center of the warm patch in a line on the y axis. Therefore, if we apply our statistical procedure over the warm patch, there are only marginal turbulent fluctuations because most of the y axis is covered by thermals. Also, over the cold patch there is a reduction of the turbulence because here there are no thermals, but only a mean sinking motion that is enclosed in the mesoscale contribution (see Fig. 2) instead of the turbulent one. An explanation of why there is more mesoscale contri-

bution in the specific humidity variance than in the temperature variance connects with the findings in the next paragraph.

Our second finding is that the total potential temperature variance peaks in the entrainment zone for case 1 (large) and case 5 (large) (see Fig. 12, top) at a value of approximately 0.18 K^2, whereas the variance of specific humidity is largely enhanced from 0.09 to 0.12 $g^2\ kg^{-2}$ due to the presence of heterogeneity. This finding could be explained by the opposing entrainment ratios of potential temperature and specific humidity. The specific humidity has in both cases a positive entrainment ratio (approximately 0.3); thus, moisture leaves the ABL and free atmospheric dry air enters. We have then a circulation in which moist air is transported upward over the warm patch and very dry air is advected downward over the cold patch (see Fig. 9). Therefore, we have, in addition to the shift from the turbulent to the mesoscale because of the fixed thermal location, an extra enhancement of the mesoscale variance in the entrainment zone, caused by a large horizontal fluctuation of specific humidity. Consequently, the total variance also increases. In this situation, the induced heterogeneous circulation contributes significantly to the variance and a stronger heterogeneity amplitude yields a larger mesoscale variance if the circulation enhances. Many boundary layer cloud parameterizations in large-scale models assume a relation between specific humidity variance and cloud cover (Teixeira and Hogan 2002); thus, heterogeneity may play a role here.

On the other hand, potential temperature has a negative entrainment ratio (-0.2); thus, air colder than the free atmosphere leaves the ABL and is replaced by warmer air. In consequence, the circulation is characterized by rising warm thermals over the warm patch and sinking warm air over the cold patch. Therefore, the mesoscale contribution is independent of the heterogeneity amplitude, because stronger thermals are compensated for by faster downward motions (see the difference between the wind vectors in cases 2 and 5 in Fig. 2) and the total variance will not exceed the homogeneous case.

These results can be related to the studies of Jonker et al. (1999) and De Roode et al. (2004), which show that the maximum spatial scales in the variances of heat, moisture, and scalars that can develop in the homogeneous ABL are determined by the entrainment ratio. They also found that for the typical -0.2 ratio of the surface and entrainment potential temperature flux, the variability is bounded and large-scale fluctuations cannot develop. On the other hand, for scalars with a positive ratio, such as specific humidity in our case, larger-scale fluctuations can develop and increase the variance. Although this is only a qualitative connection, a future study should address the development of scale levels in the heterogeneously forced ABL.

4. Summary and conclusions

We investigated the effect of heterogeneous forcings on the potential formation of convective clouds using relative humidity as an indicator. This was done by analyzing numerical experiments using a large-eddy simulation model. A sensitivity analysis was performed on the heterogeneity amplitude and the inversion strengths of potential temperature and specific humidity for a land surface that is heterogeneous in the meso-γ scale (2–20 km). The cases are integrated for 4 h, of which the last hour was used to record statistics. We analyzed the height of the ABL and the specific and relative humidity structure near the ABL top for a free convective boundary layer forced by a sensible and latent heat flux that added up to 360 W m^{-2} for all simulations. The land surface was divided into two patches, one with a low Bowen ratio (cold patch) and one with a high Bowen ratio (warm patch). Different heterogeneity amplitudes were simulated by varying the difference between the Bowen ratios of the two patches.

An analysis of entrainment and ABL growth of the heterogeneously forced ABL indicated that under heterogeneous conditions the ABL increases over the warm patch, and decreases over the cold patch. The greater ABL heights over the warm patch lead to lower absolute temperatures over the center of the warm patch. Because of the mesoscale circulation that is induced by the heterogeneous forcings, moisture is advected to the center of the warm patch. Low absolute temperatures in combination with high specific humidity over the warm patch lead to a situation in which relative humidity is higher under heterogeneous conditions than under homogeneous forcings. These are the first indications in this study that cloud formation may be favorable over the warm patches of a heterogeneous landscape.

The comparison of vertical heat flux profiles of homogeneous and heterogeneous cases sharing the same area-averaged forcings revealed that entrainment in low-amplitude heterogeneous cases appears to be less than in homogeneous cases, whereas the entrainment of large-amplitude cases exceeds the entrainment of homogeneous cases. Nevertheless, this finding is rejected by the analysis of the time evolution of the ABL height because identical entrainment velocities are found here for all cases.

The analysis of the scale levels involved in the heat

transport showed us that the entrainment heat flux consists of a mesoscale and a turbulent part. This is explained by the fact that strong entrainment events are closely linked to the mesoscale motion and are always at the same location. A larger heterogeneity amplitude leads to an increased contribution of the mesoscale motions to entrainment.

Mean vertical profiles of relative humidity are very similar in all cases, but the variability in the time-averaged RH near the top of the ABL (RH_{zi}) is greatly enhanced by the presence of heterogeneity. This finding is proven to be true for all cases with strong and weak potential temperature inversions and with moist and dry upper atmospheres. In all situations, the RH_{zi} over the warm patch is larger than over the cold patch and is also larger than in homogeneous conditions. By conditionally sampling the data, we show that thermals over heterogeneous surface conditions are more effective in transporting moisture upward because of their larger volume to surface ratio. In addition, the RH cross sections show that dry air that is entrained is transported downward mostly over the cold patch, and low values of RH are found over this patch. In cases with a drier free atmosphere, these effects can be more pronounced and dry entrainment events extend to the land surface. Therefore, we conclude that the mean RH profile shows incomplete information with regard to RH modifications by heterogeneity. It is highly relevant to calculate the variability of RH as a function of the amplitude of the heterogeneity because this variable contains the influence of heterogeneity on the maximum RH that occurs in the domain. The variances of potential temperature and specific humidity also contain the spatial variability and show a shift of the variances from the turbulent to the mesoscale. Heterogeneous forcings enhance the total variance of specific humidity, whereas the total variance of potential temperature does not increase, which is explained by the entrainment ratio.

All of the above findings suggest that land surface heterogeneity plays a significant role in the structure and value of RH_{zi}. Cloud formation may be enhanced over heterogeneous landscapes because the maximum RH and the specific humidity variance in the entrainment zone are larger than in homogeneous conditions.

Acknowledgments. The authors acknowledge the helpful comments of Ned Patton, Stephan de Roode, and Joel Schröter. This study was supported by a grant from the Netherlands Organisation for Scientific Research (NWO TopTalent). This work was sponsored by the National Computing Facilities (NCF project SG132).

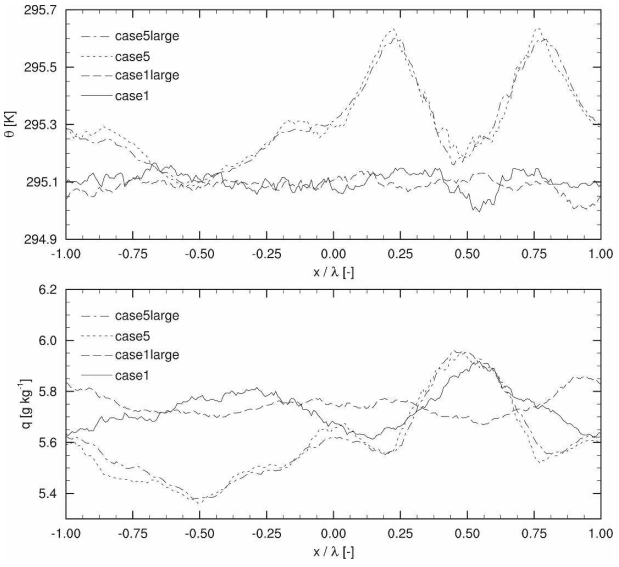

FIG. A1. 1-h time-averaged (top) potential temperatures and (bottom) specific humidities along the x axis for case 1 and case 1 (large) and case 5 and case 5 (large). Horizontal coordinates are scaled by the patch size λ.

APPENDIX

Sensitivity to Domain Size

This appendix shows the sensitivity of our results to the size of our domain. For the homogeneous case we analyzed, if the horizontal fluctuations that we found in the time-averaged potential temperature and specific humidity are the result of the limited size of the y axis, then our local average is not accurate enough. For the heterogeneous case, we tested for the same variables the sensitivity to the number of patches in our domain. We carried out the analysis on cases 1 and 5 for a domain that has 512 cells in the x axis instead of 256, thereby creating case 1 (large) and case 5 (large). Consequently, the domain on the x axis is 12 800 m instead of 6400 m and case 5 (large) has 4 patches instead of 2. We use the same statistical procedures to create statistics for 256 cells on the x axis, but the local average (see section 2c) is now computed using the average of all cells on the y axis for that specific location and all values on the y axis for the cell at the same height, but shifted 256 grid cells in positive x direction. For instance, a local mean calculated at grid cell $x = 1$, $z = 1$ is the mean of all cells in the y direction for $x = 1$, $z = 1$ and $x = 257$, $z = 1$. All of these cells have exactly the same surface forcings.

Figure A1 shows the time-averaged potential temperature and specific humidity during the hour of recording for the four cases. Case 5 and case 5 (large) yield identical profiles for both variables, with minima

of 295.1 K at $x/\lambda = -0.5$ and 0.5 and two maxima of 295.6 K at $x/\lambda = 0.25$ and 0.75. Therefore, our chosen domain setup of two patches resolves the heterogeneous cases correctly. On the other hand, the homogeneous case improves considerably when the local average is based on a greater number of points because the profile converges to a straight line (295.1 K for potential temperature and 5.75 g kg^{-1} for specific humidity), which we would expect for a case with identical surface forcings over the whole domain.

REFERENCES

Avissar, R., and Y. Liu, 1996: Three-dimensional numerical study of shallow convective clouds and precipitation induced by land surface forcing. *J. Geophys. Res.,* **101,** 7499–7518.

——, and T. Schmidt, 1998: An evaluation of the scale at which ground-surface heat patchiness affects the convective boundary layer using large-eddy simulations. *J. Atmos. Sci.,* **55,** 2666–2689.

Bretherton, C. S., and Coauthors, 1998: An intercomparison of radiatively driven entrainment and turbulence in a smoke cloud, as simulated by different numerical models. *Quart. J. Roy. Meteor. Soc.,* **125,** 391–423.

Chagnon, F. J. F., and R. L. Bras, 2005: Contemporary climate change in the Amazon. *Geophys. Res. Lett.,* **32,** L13703, doi:10.1029/2005GL022722.

——, ——, and J. Wang, 2004: Climatic shift in patterns of shallow clouds over the Amazon. *Geophys. Res. Lett.,* **31,** L24212, doi:10.1029/2004GL021188.

Crook, N. A., 1996: Sensitivity of moist convection forced by boundary layer processes to low-level thermodynamic fields. *Mon. Wea. Rev.,* **124,** 1767–1785.

Cuijpers, J. W. M., and P. G. Duynkerke, 1993: Large-eddy simulation of trade-wind cumulus clouds. *J. Atmos. Sci.,* **50,** 3894–3908.

De Roode, S. R., P. G. Duynkerke, and H. J. J. Jonker, 2004: Large-eddy simulation: How large is large enough? *J. Atmos. Sci.,* **61,** 403–421.

Dosio, A., J. Vilà-Guerau de Arellano, A. A. M. Holtslag, and P. J. H. Builtjes, 2005: Dispersion of a passive tracer in buoyancy- and shear-driven boundary layers. *J. Appl. Meteor.,* **42,** 1116–1130.

Ek, M. B., and L. Mahrt, 1994: Daytime evolution of relative humidity at the boundary layer top. *Mon. Wea. Rev.,* **122,** 2709–2721.

——, and A. A. M. Holtslag, 2004: Influence of soil moisture on boundary layer cloud development. *J. Hydrometeor.,* **5,** 86–99.

Freedman, J. M., D. R. Fitzjarrald, K. E. Moore, and R. K. Sakai, 2001: Boundary layer clouds and vegetation–atmosphere feedbacks. *J. Climate,* **14,** 180–197.

Hadfield, M. G., W. R. Cotton, and R. A. Pielke, 1991: Large-eddy simulations of thermally forced circulation in the convective boundary layer. Part I: A small-scale circulation with zero wind. *Bound.-Layer Meteor.,* **57,** 79–114.

Hechtel, L. M., C.-H. Moeng, and R. B. Stull, 1990: The effects of nonhomogeneous surface fluxes on the convective boundary layer: A case study using large-eddy simulation. *J. Atmos. Sci.,* **47,** 1721–1741.

Hussain, A. K. M. F., and W. C. Reynolds, 1970: The mechanics of an organized wave in turbulent shear flow. *J. Fluid Mech.,* **41,** 241–258.

Jonker, H. J. J., P. G. Duynkerke, and J. W. M. Cuijpers, 1999: Mesoscale fluctuations in scalars generated by boundary layer convection. *J. Atmos. Sci.,* **56,** 801–808.

Kang, S.-L., K. J. Davis, and M. LeMone, 2007: Observations of the ABL structures over a heterogeneous land surface during IHOP_2002. *J. Hydrometeor.,* **8,** 221–244.

Letzel, M. O., and S. Raasch, 2003: Large-eddy simulation of thermally induced oscillations in the convective boundary layer. *J. Atmos. Sci.,* **60,** 2328–2341.

Lilly, D. K., 2002: Entrainment into mixed layers. Part I: Sharp-edged and smoothed tops. *J. Atmos. Sci.,* **59,** 3340–3352.

Mahrt, L., 2000: Surface heterogeneity and vertical structure of the boundary layer. *Bound.-Layer Meteor.,* **96,** 33–62.

Moeng, C.-H., 1984: A large-eddy-simulation model for the study of planetary boundary layer turbulence. *J. Atmos. Sci.,* **41,** 2052–2062.

Nieuwstadt, F. T. M., and R. A. Brost, 1986: The decay of convective turbulence. *J. Atmos. Sci.,* **43,** 532–546.

Patton, E. G., P. P. Sullivan, and C. H. Moeng, 2005: The influence of idealized heterogeneity on wet and dry planetary boundary layers coupled to the land surface. *J. Atmos. Sci.,* **62,** 2078–2097.

Pielke, R. A., 2001: Influence of the spatial distribution of vegetation and soils on the prediction of cumulus convective rainfall. *Rev. Geophys.,* **39,** 151–178.

Pino, D., J. Vilà-Guerau de Arellano, and P. G. Duynkerke, 2003: The contribution of shear to the evolution of a convective boundary layer. *J. Atmos. Sci.,* **60,** 1913–1926.

Sullivan, P. P., C.-H. Moeng, B. Stevens, D. Lenschow, and S. D. Mayor, 1998: Structure of the entrainment zone capping the convective atmospheric boundary layer. *J. Atmos. Sci.,* **55,** 3042–3064.

Teixeira, J., and T. F. Hogan, 2002: Boundary layer clouds in a global atmospheric model: Simple cloud cover parameterizations. *J. Climate,* **15,** 1261–1276.

vanZanten, M. C., P. G. Duynkerke, and J. W. M. Cuijpers, 1999: Entrainment parameterization in convective boundary layers. *J. Atmos. Sci.,* **56,** 813–828.

Wicker, L. J., and W. C. Skamarock, 2002: Time-splitting methods for elastic models using forward time schemes. *Mon. Wea. Rev.,* **130,** 2088–2097.